INT. J. NUM. METH. HEAT FLUID FLOW, VOL. 3, 107–119 (1993)

TRANSIENT THERMOELASTICITY BY MULTIPLE RECIPROCITY METHOD

A. C. NEVES, L. C. WROBEL AND A. J. NOWAK†

Wessex Institute of Technology, University of Portsmouth, Ashurst Lodge, Ashurst, Southampton SO4 2AA, UK

ABSTRACT

This paper presents a boundary element formulation for transient uncoupled thermoelasticity employing a multiple reciprocity method (MRM) approximation for calculating the thermal stress field. An intermediate step, which involves curve fitting, is necessary for processing the results of the heat conduction analysis into a form suitable for the MRM. Numerical results are included which validate the present technique.

KEY WORDS Multiple reciprocity method Transient thermoelasticity Boundary element method

INTRODUCTION

In this paper, an application of the boundary element method (BEM) for transient uncoupled thermoelasticity is presented. The assumption of uncoupled thermoelasticity means that the influence of the temperature field on the stress field is taken into account but the temperature changes due to the deformation of the body are neglected[1]. Consequently, the problem can be solved in two steps: the first being the calculation of the temperature field at each time step; and the second, the stress field at the time of interest.

For the first step described above, a BEM formulation with time-dependent fundamental solutions is employed with a convolution-type time-marching scheme[2]. In this way, domain integration is avoided and high accuracy obtained.

For the second step, the multiple reciprocity method (MRM)[3] is applied to the domain integrals that appear in the BEM formulation of elasticity due to the temperature gradient. The MRM is an efficient technique for transforming the domain integral resulting from the thermal field into a series of equivalent boundary integrals. The MRM can be interpreted as a generalization of the Galerkin-tensor technique[2], and has already been successfully applied to a number of problems including calculation of eigenvalues of the Helmholtz equation[4], viscous hydrodynamics[5], thermoelasticity with steady temperature distributions[6] and neutron diffusion problems[7].

An intermediate step is required for processing the results of the heat conduction analysis into a form suitable for the use of the MRM in the stress field analysis. This involves a curve fitting procedure and calculation of the time derivatives of the temperature and heat flux along the boundary. This point is also discussed in the following text which starts with a brief description of the BEM formulations for transient thermoelasticity without internal heat sources, proceeds to the numerical implementation and presents results of analyses to validate the technique. These

†On leave from Institute of Thermal Technology, Technical University of Silesia, Gliwice, Poland.

0961–5539/93/020107–13$2.00

Received April 1992
Revised September 1992

results are compared with other BEM solutions employing cell discretization for the domain integral[8] and/or with analytical solutions when available.

PROBLEM DEFINITION

The proposed technique is applied to two-dimensional transient heat conduction problems without internal heat generation. Consider a body occupying a domain Ω with boundary Γ, for which its thermal state is governed by the diffusion equation:

$$\nabla^2 T(X,t) = \frac{1}{\kappa}\frac{\partial T(X,t)}{\partial t} \quad \text{in } \Omega \tag{1}$$

where $T(X,t)$ is the temperature at point X at time t and κ is the thermal diffusivity ($\kappa = \lambda/\rho c$, λ represents the thermal conductivity, ρ stands for density and c is the specific heat).

The imposed Dirichlet, Neumann and Robin types of boundary conditions are given respectively by:

$$T = \bar{T} \qquad \text{on } \Gamma_1 \tag{2}$$

$$q = -\lambda\frac{\partial T}{\partial n} = \bar{q} \quad \text{on } \Gamma_2 \tag{3}$$

$$q = h(T - T_s) \quad \text{on } \Gamma_3 \tag{4}$$

where q is the heat flux, h is the heat transfer coefficient and T_s is the ambient temperature.

Since the problem is time-dependent, initial conditions at time $t = t_0$ must also be prescribed, i.e.:

$$T = T_0 \quad \text{in } \Omega \tag{5}$$

Considering the time dependence of the problem, an application of the reciprocity theorem allows the differential equation (1) to be transformed to the following integral equation[9]:

$$CT_{t_F} + \kappa\int_{t_0}^{t_F}\int_{\Gamma} q^* T \, d\Gamma \, dt = \kappa\int_{t_0}^{t_F}\int_{\Gamma} T^* q \, d\Gamma \, dt - \lambda\int_{\Omega} T^* T_0 \, d\Omega \tag{6}$$

where C is a position-dependent free coefficient, t_0 is the initial time and t_F is the final time of the analysis.

The time-dependent fundamental solutions T^* and q^* are of the form:

$$T^* = \frac{1}{4\pi\kappa\tau}\exp\left(\frac{-r^2}{4\kappa\tau}\right)H(\tau) \tag{7}$$

$$q^* = -\lambda\frac{\partial T^*}{\partial n} \tag{8}$$

where $\tau = t_F - t$, $H(\tau)$ is the Heaviside function and r is the distance between the source and field points.

The numerical solution of (6) employs a convolution-type time-marching scheme. This scheme allows the domain integral in (6) to be transformed into equivalent boundary integrals if T_0 satisfies Laplace's or Poisson's equation. Constant time interpolation and linear boundary elements are used in the analysis. At each time step, results for the temperature and heat flux variations along the boundary are obtained. Temperature and fluxes at internal points can also be calculated if required. The numerical implementation of the heat conduction formulation is discussed in detail in Ref. 2.

The second part of the analysis consists in calculating the displacements and stresses at the time of interest. The problem is now governed by the Navier equation and the corresponding

integral equations for the displacements at any point and stresses at internal points are given respectively by:

$$C_{ij}u_j = \int_\Gamma u^*_{ij}p_j\,d\Gamma - \int_\Gamma p^*_{ij}u_j\,d\Gamma + 2\mu\left(\frac{1+\nu}{1-2\nu}\right)\alpha\int_\Omega u^*_{ij,j}T\,d\Omega \tag{9}$$

$$\sigma_{ij} = \int_\Gamma u^*_{ijk}p_k\,d\Gamma - \int_\Gamma p^*_{ijk}u_k\,d\Gamma - 2\mu\left(\frac{1+\nu}{1-2\nu}\right)\alpha\left[\int_\Omega \sigma^*_{ij}T\,d\Omega + T\delta_{ij}\right] \tag{10}$$

where: u_j is the displacement in the j direction; p_j is the traction in the j direction; σ_{ij} is the stress tensor at an internal point; α is the coefficient of linear thermal expansion; δ_{ij} is the Kronecker delta; ν is the Poisson's ratio; μ is the shear modulus.

The fundamental solutions of (9) and (10) are given by:

$$u^*_{ij} = \frac{1}{8\pi(1-\nu)\mu}\{(3-4\nu)\ln(1/r)\delta_{ij} + r_{,i}r_{,j} - \tfrac{1}{2}\delta_{ij}\} \tag{11}$$

$$p^*_{ij} = \frac{-1}{4\pi(1-\nu)r}\left\{[(1-2\nu)\delta_{ij} + 2r_{,i}r_{,j}]\frac{\partial r}{\partial n} - (1-2\nu)(r_{,i}n_j - r_{,j}n_i)\right\} \tag{12}$$

$$u^*_{ij,j} = \frac{-(1-2\nu)}{4\pi(1-\nu)\mu}\frac{r_{,i}}{r} \tag{13}$$

$$u^*_{ijk} = \frac{1}{4\pi(1-\nu)r}\{(1-2\nu)(r_{,j}\delta_{ik} + r_{,i}\delta_{jk} - r_{,k}\delta_{ij}) + 2r_{,i}r_{,j}r_{,k}\} \tag{14}$$

$$p^*_{ijk} = \frac{\mu}{2\pi(1-\nu)r^2}\left\{2\frac{\partial r}{\partial n}[(1-2\nu)\delta_{ij}r_{,k} + \nu(\delta_{ik}r_{,j} + \delta_{jk}r_{,i}) - 4r_{,i}r_{,j}r_{,k}]\right.$$
$$\left. + 2\nu(n_ir_{,j}r_{,k} + n_jr_{,i}r_{,k}) + (1-2\nu)(2n_kr_{,i}r_{,j} + n_j\delta_{ik} + n_i\delta_{jk}) - (1-4\nu)n_k\delta_{ij}\right\} \tag{15}$$

$$\sigma^*_{ij} = \frac{(1-2\nu)}{\pi(1-\nu)}\left[\frac{1}{r^2}\left(r_{,i}r_{,j} - \frac{\delta_{ij}}{2}\right) - \frac{\pi}{2(1-2\nu)}\delta_{ij}\Delta(\xi, x)\right] \tag{16}$$

where $\Delta(\xi, x)$ is the Dirac delta.

Equations (9) and (10) can only be solved when the temperature field resulting from (6) is known.

In order to avoid domain discretization, the multiple reciprocity method is used to transform the domain integrals of (9) and (10) into boundary integrals given by[6]:

$$\int_\Omega u^{*(0)}_{ij,j}T^{(0)}\,d\Omega = \int_\Gamma \sum_{L=0}^{\infty}\left(\frac{\partial u^{*(L+1)}_{ij,j}}{\partial n}T^{(L)} - u^{*(L+1)}_{ij,j}\frac{\partial T^{(L)}}{\partial n}\right)d\Gamma \tag{17}$$

$$\int_\Omega \sigma^{*(0)}_{ij}T^{(0)}\,d\Omega = \int_\Gamma \sum_{L=0}^{\infty}\left(\frac{\partial \sigma^{*(L+1)}_{ij}}{\partial n}T^{(L)} - \sigma^{*(L+1)}_{ij}\frac{\partial T^{(L)}}{\partial n}\right)d\Gamma \tag{18}$$

where the index (0) indicates that these are the original expressions.

The higher order fundamental solutions in (17) and (18) are given by:

$$u^{*(L+1)}_{ij,j} = \frac{-(1-2\nu)}{4\pi(1-\nu)\mu}A^{(L+1)}r^{2L+1}r_{,i}(\ln(r) - B^{(L+1)}) \tag{19}$$

$$\frac{\partial u^{*(L+1)}_{ij,j}}{\partial n} = \frac{-(1-2\nu)}{4\pi(1-\nu)\mu}A^{(L+1)}r^{2L}[(n_i + 2Lr_{,i}r_{,j}n_j)(\ln(r) - B^{(L+1)}) + r_{,i}r_{,j}n_j] \tag{20}$$

$$\sigma_{ij}^{*(L+1)} = -\frac{(1-2\nu)}{4\pi(1-\nu)} C^{(L+1)}\left[\frac{1}{1-2\nu}(\ln(r) - D^{(L+1)})\delta_{ij} + \left(r_{,i}r_{,j} - \frac{\delta_{ij}}{2}\right)(E^{(L+1)}\ln(r) - F^{(L+1)})\right] r^{2L} \tag{21}$$

$$\frac{\partial\sigma_{ij}^{*(L+1)}}{\partial n} = -\frac{(1-2\nu)}{4\pi(1-\nu)} C^{(L+1)}\left\{\frac{1}{1-2\nu}[2L(\ln(r) - D^{(L+1)}) + 1]r_{,k}n_k\delta_{ij} + \left[\left(r_{,i}r_{,j} - \frac{\delta_{ij}}{2}\right)(2L\ln(r) + 1)r_{,k}n_k + (n_i r_{,j} + n_j r_{,i} - 2r_{,i}r_{,j}r_{,k}n_k)\ln(r)\right]E^{(L+1)} - \left[2Lr_{,k}n_k\left(r_{,i}r_{,j} - \frac{\delta_{ij}}{2}\right) + (n_i r_{,j} + n_j r_{,i} - 2r_{,i}r_{,j}r_{,k}n_k)\right]F^{(L+1)}\right\} r^{2L-1} \tag{22}$$

where coefficients satisfy the following recurrence relationships:

$$A^{(L+1)} = \frac{A^{(L)}}{(2L+1)^2 - 1} \tag{23}$$

$$B^{(L+1)} = B^{(L)} + \frac{2(2L+1)}{(2L+1)^2 - 1} \tag{25}$$

$$C^{(L+1)} = \frac{C^{(L)}}{4L^2} \tag{25}$$

$$D^{(L+1)} = D^{(L)} + \frac{1}{L} \tag{26}$$

$$E^{(L+1)} = \frac{2L}{L+1} \tag{27}$$

$$F^{(L+1)} = (LF^{(L)} + E^{(L+1)})\frac{L}{L^2 - 1} \tag{28}$$

The initial values for $L = 0$ are $A^{(1)} = 1/2$, $B^{(1)} = 0$, $C^{(1)} = 1$, $D^{(1)} = 0$, $E^{(1)} = 0$ and $F^{(1)} = -1$; and for $L = 1$, $F^{(2)} = 0$.

The temperature distribution $T^{(L)}$ in (17) and (18) can be obtained from (1) by applying the recurrence formula $T^{(L+1)} = \nabla^2 T^{(L)}$ successively as follows:

$$T^{(1)} = \nabla^2 T^{(0)} = \frac{1}{\kappa}\frac{\partial T^{(0)}}{\partial t}$$

$$T^{(2)} = \nabla^2 T^{(1)} = \nabla^2\left(\frac{1}{\kappa}\frac{\partial T^{(0)}}{\partial t}\right) = \frac{1}{\kappa}\frac{\partial}{\partial t}(\nabla^2 T^{(0)}) = \frac{1}{\kappa^2}\frac{\partial^2 T^{(0)}}{\partial t^2}$$

$$\bullet$$

$$\bullet$$

$$\bullet$$

$$T^{(n)} = \frac{1}{\kappa^n}\frac{\partial^n T^{(0)}}{\partial t^n} \tag{29}$$

Similarly, the normal derivatives $\partial T^{(L)}/\partial n$ can be obtained from (3) as follows:

$$\frac{\partial T^{(0)}}{\partial n} = -\frac{q^{(0)}}{\lambda}$$

$$\frac{\partial T^{(1)}}{\partial n} = \frac{\partial}{\partial n}\left(\frac{1}{\kappa}\frac{\partial T^{(0)}}{\partial t}\right) = \frac{1}{\kappa}\frac{\partial}{\partial t}\left(\frac{\partial T^{(0)}}{\partial n}\right) = -\frac{1}{\kappa\lambda}\frac{\partial q^{(0)}}{\partial t}$$

$$\bullet$$

$$\bullet$$

$$\bullet$$

$$\frac{\partial T^{(n)}}{\partial n} = -\frac{1}{\kappa^n\lambda}\frac{\partial^n q^{(0)}}{\partial t^n} \tag{30}$$

SOLUTION PROCEDURES

Figure 1 schematizes the solution procedures of a transient thermoelastic problem using two different boundary element approaches for the stress analysis: the first one (CELL) is based on cell discretization and requires from the first part (BEM2C) the temperature distribution all over the domain Ω at the time of interest t_i while in the second approach (MRM), the multiple reciprocity method is used and only the boundary needs to be discretized. The results of both approaches are then compared.

The MRM requires an intermediate analysis (LSM) in order to obtain the Laplacians of temperature and their normal derivatives as shown in (29) and (30). This analysis consists of fitting the values of $T^{(0)}$ and $q^{(0)}$ at each node on the boundary Γ at 'm' different time levels near the time of interest 't_i' by polynomial functions of degree 'n' given by:

$$\mathscr{T}_\Gamma^{(0)}(t_i) = \sum_{N=0}^{n} a_N T_\Gamma^{(0)N}(t_{i1} \cdots t_{im}) \tag{31}$$

$$\mathscr{Q}_\Gamma^{(0)}(t_i) = \sum_{N=0}^{n} b_N q_\Gamma^{(0)N}(t_{i1} \cdots t_{im}) \tag{32}$$

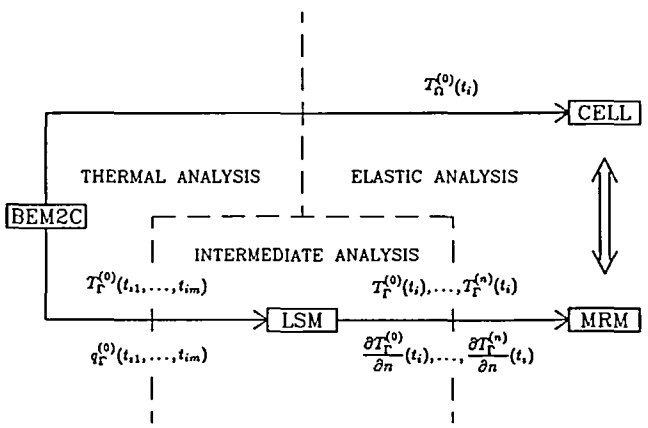

Figure 1 Solution procedures

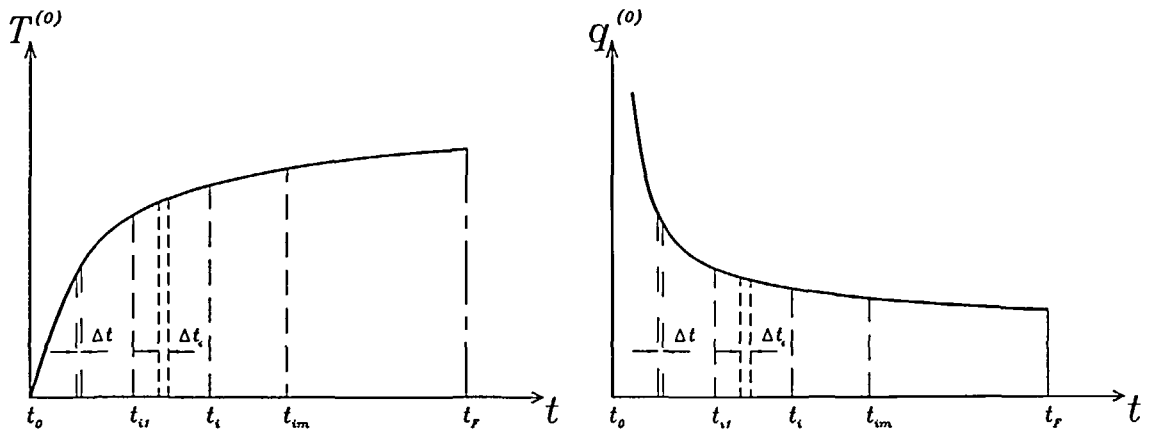

Figure 2 Temperature and flux variations with time for a particular node

where t_{i1} and t_{im} are respectively the initial and final time of the range containing m different levels near the time of interest t_i (*Figure 2*).

The coefficients a_N and b_N in the previous equations are calculated by using a least square method with LU decomposition[10]; then, the n derivatives with respect to the time of interest t_i can be easily found in order to calculate $T^{(L)}$ and $\partial T^{(L)}/\partial n$ according to (29) and (30). Note that the series in (17) and (18) become finite summations of '$n + 1$' terms.

For better results, it is suggested that a significant range of time around the time of interest be selected, such that t_i is located near the centre of the interval $t_{im} - t_{i1}$.

The next section presents three different examples to illustrate the numerical implementation of transient problems by MRM and cells integration.

NUMERICAL EXAMPLES

Example 1: infinite slab

In the first example, a quarter of a rectangular plate with zero initial temperature submitted to the Dirichlet boundary condition $T = 1$ along the faces $x = \pm 5$ and Neumann condition $q = 0$ along the faces $y = \pm 4$ is analysed (*Figure 3*). This is equivalent to the one-dimensional problem of an infinite slab over both faces of which a temperature is prescribed. The analytical solution for the temperature distribution is given elsewhere[9,11].

The first part of the analysis provides the temperature and normal flux distributions considering a time step of 0.5. It was noted that the steady state is reached at approximately $t = 30$. It was also noted that the results for BEM2C are less accurate for the initial time steps because of the common difficulty of modelling thermal shocks. However, they quickly improve after a few time steps.

The ranges selected for the process of curve fitting (LSM) are shown in *Table 1*. For all the times of interest, a polynomial of degree $n = 7$ was used to fit the values of $T^{(0)}$ and $q^{(0)}$ at $m = 10$ different time levels with a time step of 1.

It can be noted that these ranges are generally centred at the time of interest apart from the time $t_i = 5$. In this case, the range is shifted to higher times in order to avoid in the fitting process the inaccurate data resulting from the first analysis for early times and the sharp variations in the temperature and heat flux which are difficult to reproduce with a polynomial.

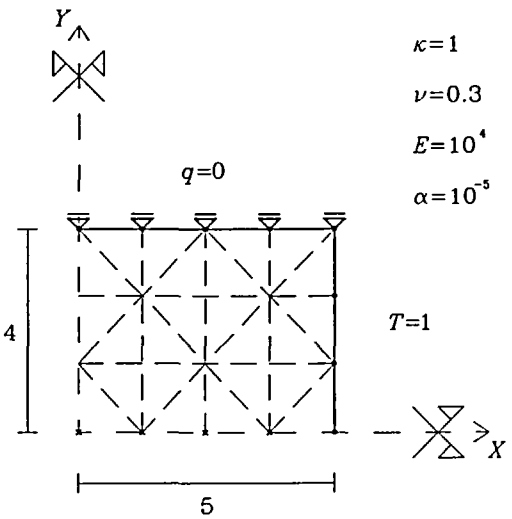

Figure 3 Discretization of the infinite slab

Table 1 Time range for different times of interest

Time of interest, t_i	Initial time, t_{i1}	Final time, t_{im}	Time step, Δt_i
5	3	12	1
10	6	15	1
15	11	20	1
20	16	25	1

Table 2 Stresses σ_y along X axis for different times of interest

Time	Coord X	Analytical solution	Analytical input		Numerical input	
			CELL	MRM	CELL	MRM
	0.00	−0.0228	−0.0227	−0.0226	−0.0224	−0.0228
	1.25	−0.0284	−0.0283	−0.0282	−0.0280	−0.0283
5	2.50	−0.0447	−0.0446	−0.0445	−0.0443	−0.0448
	3.75	−0.0698	−0.0698	−0.0702	−0.0695	−0.0724
	5.00	−0.1000	−0.1002	−0.1009	−0.1001	−0.1034
	0.00	−0.0525	−0.0525	−0.0525	−0.0525	−0.0534
	1.25	−0.0562	−0.0561	−0.0561	−0.0561	−0.0570
10	2.50	−0.0664	−0.0664	−0.0664	−0.0664	−0.0671
	3.75	−0.0818	−0.0818	−0.0818	−0.0818	−0.0822
	5.00	−0.1000	−0.1001	−0.1001	−0.1000	−0.1002
	0.00	−0.0710	−0.0710	−0.0710	−0.0711	−0.0718
	1.25	−0.0732	−0.0732	−0.0732	−0.0733	−0.0739
15	2.50	−0.0795	−0.0795	−0.0795	−0.0796	−0.0801
	3.75	−0.0889	−0.0889	−0.0889	−0.0889	−0.0893
	5.00	−1.0000	−0.1001	−0.1001	−0.1000	−0.1002
	0.00	−0.0823	−0.0823	−0.0823	−0.0824	−0.0829
	1.25	−0.0837	−0.0836	−0.0836	−0.0837	−0.0842
20	2.50	−0.0875	−0.0875	−0.0875	−0.0875	−0.0879
	3.75	−0.0932	−0.0932	−0.0932	−0.0932	−0.0935
	5.00	−0.1000	−0.1000	−0.1001	−0.1000	−0.1001

Different ranges and degrees of the curve fitting function were tested but the results changed only slightly. So, the values in *Table 1* appear to be satisfactory in the present case.

The thermal stress field is obtained using both cells integration and the MRM approach. *Table 2* compares the stresses σ_y along the X axis for different times of interest. The third column presents the analytical solution for σ_y given earlier[1,11]. The next two columns show the same quantity obtained by using the CELL and MRM approaches in the second part of the analysis,

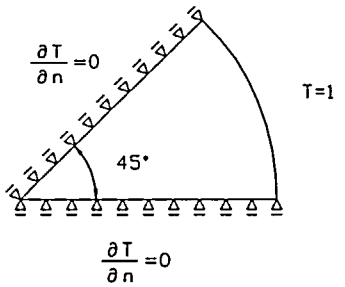

Figure 4 Discretization of the solid disc

Table 3 Fluxes at $R = 1$ for different times

Time	q_{anal}	$q_{0.005}$	$q_{0.001}$
0.01	5.098	6.805	5.417
0.02	3.466	4.008	3.551
0.03	2.728	2.995	2.765
0.04	2.286	2.446	2.305
0.05	1.983	2.090	1.994
0.06	1.758	1.832	1.764
0.07	1.582	1.637	1.586
0.08	1.434	1.482	1.441
0.09	1.320	1.354	1.321
0.10	1.218	1.246	1.218
0.15	0.861	0.872	0.858
0.20	0.634	0.638	—
0.25	0.472	0.473	—
0.30	0.353	0.353	—
0.35	0.264	0.264	—
0.40	0.198	0.198	—
0.45	0.148	0.148	—
0.50	0.111	0.111	—

respectively. In this case, both approaches use the temperature and flux distributions calculated analytically at different time levels, instead of numerically. Finally, the last two columns present the stresses σ_y obtained by using the CELL and MRM approaches with the values of temperature and flux provided by the first part of the numerical analysis (BEM2C).

For the case where Laplacians of temperatures and heat flux were calculated from analytical input, the results obtained from both approaches were very accurate. This proves the correctness of the MRM approach and the curve fitting used. For the case when the series of Laplacians was calculated from numerical data provided by BEM2C, the results of thermal stresses obtained with the cell approach were slightly better. This is generally a consequence of the BEM2C analysis which produces more accurate temperatures at internal points than along the boundary, as well as less accurate heat fluxes on the boundary, especially near the corners.

Example 2: solid disc

In this example, transient thermal stresses in a solid disc of unit radius are investigated. The disc has zero initial temperature and, at time zero, the temperature of the external edge is suddenly elevated and maintained at unit value.

Figure 4 presents the discretization and boundary conditions of one-eighth of the disc using 28 linear boundary elements. The non-dimensionalized material properties for the plane stress analysis are $\rho c = 1$, $\kappa = 1$, $\nu = 0.333$, $E = 1.333$ and $\alpha = 0.75$.

Table 3 compares the analytical values of the heat flux[9] at the outer edge for different times with the numerical results obtained by running the program BEM2C twice using different time steps: in the first run, the flux was calculated at each of the 100 steps of $\Delta t = 0.005$ while in the second one, 150 steps of $\Delta t = 0.001$ were considered. It can be seen that the first run provides inaccurate fluxes for $t < 0.10$. So, for these times of interest the results of the second run were used instead. However, considerable disturbances are expected in the thermal stresses when the values of the temperature and heat flux on the boundary for $t < 0.04$ are used in the fitting process.

The temperature variations for different radial distances, obtained from the first run are plotted in *Figure 5*. The error is less than 1% even for short times.

For the curve fitting process, different time ranges listed in *Table 4* were used. For each time of interest, a polynomial of degree $n = 7$ and a time step $\Delta t_i = 0.1$ were employed.

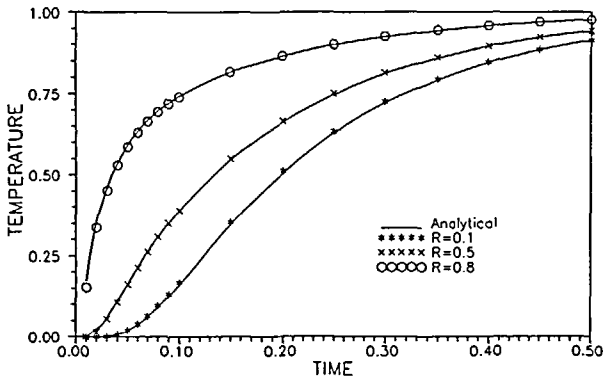

Figure 5 Temperature variations for different values of R

Table 4 Time range for different times of interest

Time of interest, t_i	Time levels, m	Initial time, t_{i1}	Final time, t_{im}
0.05	10	0.03	0.12
0.06	10	0.03	0.12
0.07	10	0.03	0.12
0.08	10	0.04	0.13
0.09	10	0.05	0.14
0.10	10	0.06	0.15
0.15	20	0.06	0.25
0.20	20	0.11	0.30
0.25	20	0.16	0.35
0.30	20	0.21	0.40
0.35	20	0.26	0.45
0.40	20	0.31	0.50

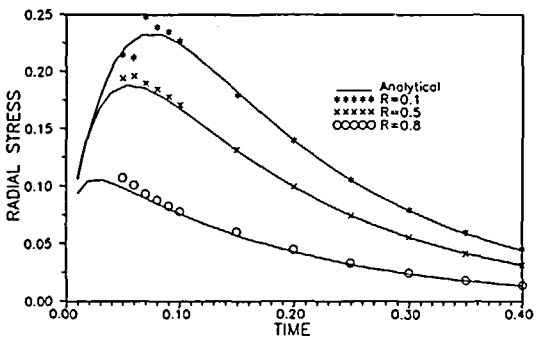

Figure 6 Radial stresses in the solid disc

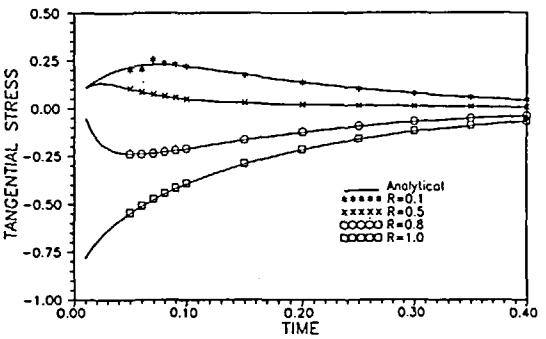

Figure 7 Tangential stresses in the solid disc

As in the previous example, apart from the early times, all other times of interest are centred in the respective range.

The radial and tangential stresses at different radii R obtained from the MRM program for several times of interest are compared with the analytical solution[12] in *Figures 6* and *7* respectively.

Regarding the convergence of the series, it was noticed that the smaller the value of r and the smoother the variation of T and q with time, the quicker the series converges. For the discretization used, the most critical point occurs when the source point is located near the centre of the disc and the field point along the external boundary. In this case $r = r_{max} = R_0$ and the variation of q on the boundary is very strong, specially at early times. This is the reason why good results were not obtained for early times, particularly when the source point is located near the centre of the disc.

The same example was analysed using eight linear elements over one quarter of the disc and considering the double symmetry of the problem. In this case, however, the convergence of the series was much weaker since $r_{max} = 2R_0$. Consequently, acceptable results were obtained only for $t > 0.30$ and using a high order polynomial. In order to investigate this behaviour, the MRM program was run with $T^{(L)}$ and $\partial T^{(L)}/\partial n$ calculated analytically and the numerical results for the tangential stress at the boundary are compared with the analytical ones in *Table 5*. It can be seen that even for the early times the series in (17) and (18) converge although a large number of terms was required.

Table 5 Number of terms used to obtain convergent σ_θ results for each time of interest

Time of interest	Number of terms	σ_θ analy.	σ_θ numer.
0.01	48	−0.7842	−0.7763
0.05	40	−0.5477	−0.5433
0.10	28	−0.3941	−0.3911
0.20	16	−0.2178	−0.2162
0.30	10	−0.1220	−0.1211

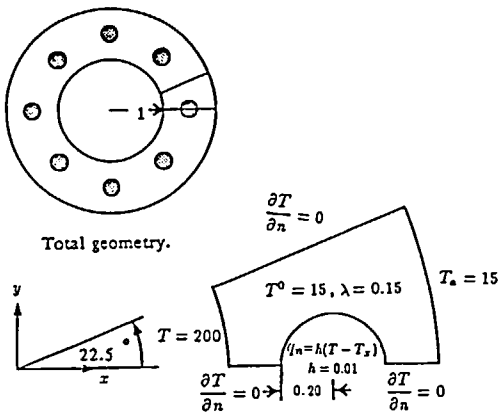

Figure 8 Geometry of the cooling cylinder

The slow convergence requires additional terms in the series which are very difficult to be accurately represented by the corresponding time derivative of the higher order polynomial used in the fitting process. It is suggested that the data from BEM2C analysis could be fit by another function which better accounts for thermal shocks, e.g. an error function or an incomplete gamma function.

Example 3: heat conduction in a cooling cylinder

Consider a thick circular cylinder with internal and external radii of 1 cm and 2 cm respectively, cooled by eight ducts with radius 0.2 cm. *Figure 8* shows a cross-section of the cylinder. Due to the symmetry, only 1/16 of the cooling cylinder is analysed.

The material constants are $\rho c = 1$ W.sec/(cm^3.°C), $\lambda = 0.15$ W/(cm.°C), $\nu = 0.3$, $E = 2.07 \times 10^5$ N/cm^2 and $\alpha = 10^{-5}$ °C^{-1}. The temperatures along the inner and outer faces of the cylinder are kept constant at 200°C and 15°C, respectively. The cylinder is cooled through the surface of the cooling ducts by water at $T_s = 20$°C with $h = 0.01$ W/(cm^2.°C). At the time $t = 0$, the temperature of the cylinder is $T_0 = 15$°C. To avoid the domain integral of (6), the initial temperature is subtracted from the temperature field, and is then added at the end of the first part of the analysis.

In this boundary element analysis, only 68 linear elements were used. The results of the first part of the analysis were compared with a finite element solution employing 1344 triangular elements[13], while the results of the second part were compared with another boundary element approach based on cell discretization using 68 linear elements and 302 triangular cells. *Figure 9* shows the discretization of the problem for the different approaches.

In the finite element approach, a time increment $\Delta t = 0.01$ sec was adopted. In the case of boundary elements, it was noted that decreasing the time step improves the results significantly for short times and only slightly for long times, while, on the other hand, it also increases the computational effort. For this reason, it was decided to use different time increments depending on the time of interest (*Table 6*).

Figure 10 compares the isotherms at different times of interest obtained by using the finite element and boundary element methods. In this example, the steady state is reached at $t = 8.0$ sec.

For the curve fitting, the range selected for $t_i = 0.6$ sec was from $t_{i1} = 0.28$ sec to $t_{im} = 1.16$ sec with $\Delta t_i = 0.08$ sec; and for $t_i = 6.0$ sec, $t_{i1} = 4.4$ sec and $t_{im} = 8.0$ sec with $\Delta t_i = 0.4$ sec. A polynomial of degree $n = 7$ was used. Varying the time range or the degree of the polynomial did not change the results significantly.

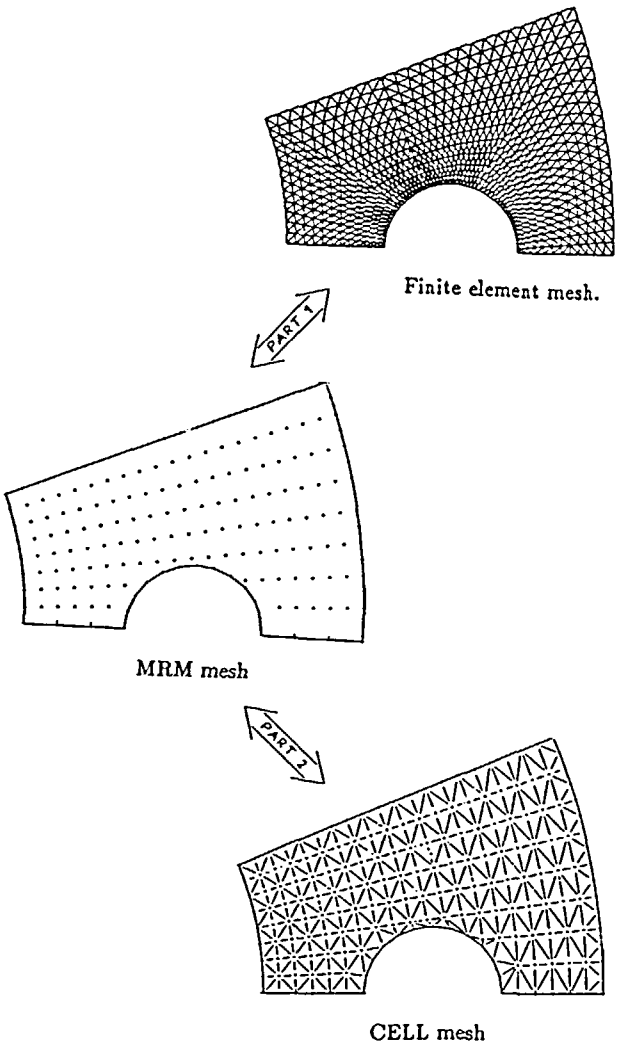

Figure 9 Discretization of the cooling cylinder

Table 6 Time range for different times of interest

Time of interest	Initial time	Final time	Time step
0.06	0	0.12	0.002
0.60	0	1.20	0.020
6.00	0	8.00	0.200

In the second part of the analysis, the results from the MRM approach are compared with the cell approach. The contour plots in *Figure 11* show the good agreement between the MRM and CELL solutions for the von Mises stresses at the times of interest $t = 0.6$ sec and $t = 6.0$ sec.

The MRM failed to produce reasonable results for the early time $t = 0.06$ sec, although several

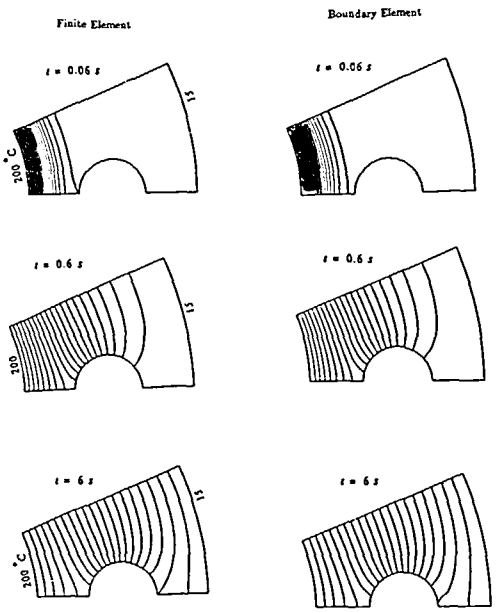

Figure 10 Isotherms for different times of interest

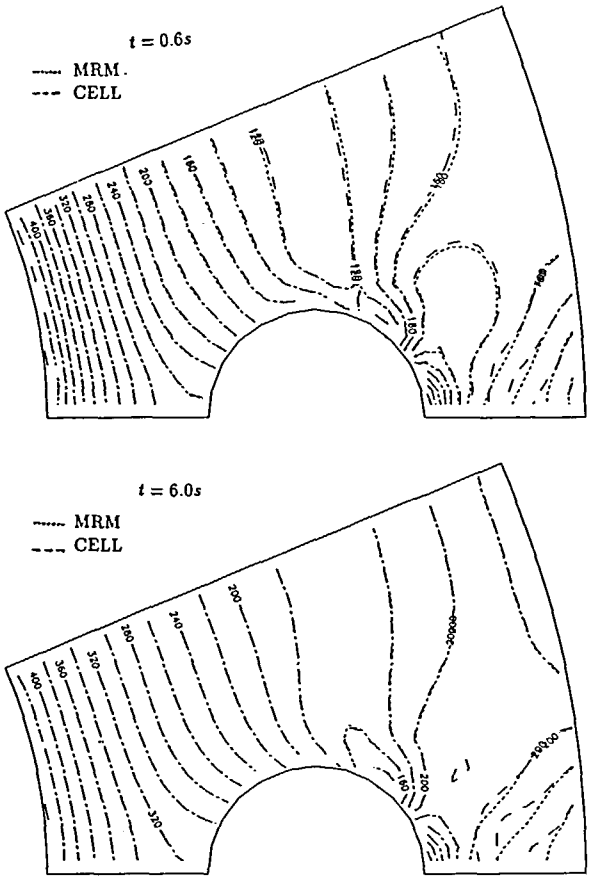

Figure 11 von Mises stresses for different times of interest

different time ranges and polynomial degrees were tested. The main reason is the slow convergence of the series caused by the very sharp temperature gradients which appear at the beginning of the process. The discussion about convergence, given in the previous example, is also valid for the present case.

CONCLUSION

This paper presented an application of the multiple reciprocity method to obtain a boundary-only formulation for the analysis of two-dimensional transient uncoupled thermoelastic problems.

The MRM is used for calculating the stress field and requires an intermediate step in which, for each boundary node, the temperature and flux variations with time are fitted by polynomial functions, and their time derivatives calculated at the time of interest. It is suggested that a significant range of time around the time of interest be selected. It was noted that the higher the order of the polynomials, the better the results. However, they require more computing time and data storage and also may cause roundoff error due to multiplication of large values by small ones. The examples show that the results are in good agreement with analytical solutions and another boundary element formulation based on cell discretization for the case where the

temperature and flux variation are well-behaved. However, the present formulation did not produce reasonable results for sharp variations of the heat flux, i.e. near the thermal shock. This is a consequence of the slow convergence of the series, which requires more terms. These additional terms are difficult to represent by the derivatives of the higher order polynomial used to fit the results of the first analysis.

ACKNOWLEDGEMENT

The first author would like to thank CNPq (Brazilian Scientific Research Council) for financial support.

REFERENCES

1 Boley, B. A. and Weiner, J. H. *Theory of Thermal Stresses*, John Wiley, New York (1960)
2 Brebbia, C. A., Telles, J. C. F. and Wrobel, L. C. *Boundary Element Techniques: Theory and Applications in Engineering*, Springer-Verlag, Berlin (1984)
3 Nowak, A. J. and Brebbia, C. A. The multiple-reciprocity method. A new approach for transforming BEM domain integrals to the boundary, *Eng. Anal. Boundary Elements*, **6** (3), 164–168 (1989)
4 Kamiya, N. and Andoh, E. Robust boundary element scheme for Helmholtz eigenvalue equation, in *BEM XIII* (Ed. C. A. Brebbia and G. S. Gipson), Comp. Mech. Publ., Southampton (1991)
5 Power, H. and Power, B. F. Solving Ossen's system of equations by boundary elements using multiple reciprocity method, *Eng. Anal. Boundary Elements*, **10** (1), 69–74 (1992)
6 Neves, A. C. and Nowak, A. J. Steady-state thermoelasticity by multiple reciprocity method, *Int. J. Num. Meth. Heat Fluid Flow*, **2**, 429–440 (1992)
7 Itagaki, M. and Brebbia, C. A. Multiple reciprocity boundary element formulation for one-group fission neutron source iteration problems, *Eng. Anal. Boundary Elements*, **10** (4), 345–352 (1992)
8 Telles, J. C. F. and Brebbia, C. A. On the application of boundary element method in plasticity, in *New Developments in Boundary Element Methods* (Ed. C. A. Brebbia), CMP, Southampton, pp. 295–317 (1980)
9 Carslaw, H. S. and Jaeger, J. C. *Conduction of Heat in Solids*, 2nd Edn, Clarendon Press, Oxford (1959)
10 Press, W. H., Flannery, B. P., Teukolsky, S. A. and Vetterling, W. T. *Numerical Recipes*, Cambridge University Press, Cambridge (1986)
11 Sladek, V. and Sladek, J. Computation of thermal stresses in quasi-static non-stationary thermoelasticity using boundary elements, *Int. J. Num. Meth. Eng.*, **28**, 1131–1144 (1989)
12 Timoshenko, S. P. and Goodier, J. N. *Theory of Elasticity*, McGraw-Hill, New York (1970)
13 Ninomiya, H. and Onishi, K. *Flow Analysis Using a PC*, CRC Press and Comp. Mech. Publ., Southampton (1991)